Colloid Polym Sci 273:1008–1021 (1995)

ORIGINAL CONTRIBUTION

S. Kreitmeier
M. Wittkop
T. Wagner
D. Göritz
R. Zietz

Investigations of hard elastic polypropylene with respect to the coil-strand-transition model

Received: 10 April 1995
Accepted: 9 June 1995

Dr. S. Kreitmeier (✉) · M. Wittkop
T. Wagner · D. Göritz
Universität Regensburg
Institut für Experimentelle und
AngewandtePhysik
93040 Regensburg, Germany

R. Zietz
DKI Darmstadt
c/o DESY-HASYLAB Hamburg

Abstract Hard elastic polypropylene was investigated by x-ray scattering using synchrotron radiation and by performing stress strain measurements in different liquids. It was found that the long period increases with elongation up to $\lambda \approx 1.3$–1.4. Beyond this extension a change in the deformation behavior takes place. In the range from $\lambda \approx 1.1$ to $\lambda \approx$ 1.3–1.4 the deformation measurements in the different liquids are in good agreement with the coil-strand-transition model. The proposed linear relationship between the deformation work and the elongation could be confirmed. The same holds for the surface energy. Moreover, the calculated ratio between the surface energy and the deformation work agrees with the measurements.

Key words Hard elastic polymers – x-ray scattering – deformation behavior – liquids – surface tension – inhomogeneous deformation

Introduction

In the 1960s hard elastic materials were developed by Celanese [1]. These materials showed interesting properties like high elastic recovery combined with high tension in a temperature regime ranging from far below the glass transition to well above. This gave rise to a lot of investigations. Noether et al. [2–5] proved the elastic behavior of melt spun polymers and made first x-ray defraction experiments to explain the morphology. Garber and Clark [6, 7], Quynn and Brody [8] as well as Sprague [9] presented first models. An overview on the properties of different materials was given in the articles of Sprague [9] and Cannon et al. [10]. A superstructure of lamellae each perpendicular to the drawing direction should act as leaf springs or coil springs. Bending of lamellae should deliver the retractive forces. TEM investigations made by Noether, Whitney, Hay, Petermann, Cayrol, Gleiter, Miles, Adams et al. [2, 5, 11–14] showed that many fibrils and voids are formed between the lamellae in the amorphous regions. According to Petermann, Cayrol, Gleiter, Miles and Adams the retractive force should be due to the elastic properties of these fibrils. Similar to that, Göritz and Müller [15, 16] suggested that entropic changes resulting from the formation of fibrils are the reasons for the elastic recovery. Wool [17] noted that energetic effects (adhesive fraction and beam deflection) must dominate the deformation. Hosemann and co-workers [18, 19] stressed microparacrystalline effects to explain the retractive force. Investigating hard elastic polyethylene, Hashimoto et al. [20] interpreted the residual strain in the bulk in terms of irreversible deformation of submicroscopic structures, i.e., lamellae. They discussed as possible mechanism of irreversible lamellar deformation chain slippage within lamellae, lamellar destruction, and destruction of lamellar tie links. According to Ishikawa et al. [21] the elastic deformation is based on an increase of intermolecular distances against van der Waals forces and on changes of bond and rotation angles in the molecules.

Baer and co-workers [22, 23] found that profusely crazed, glassy, high-impact polystyrene also exhibits hard

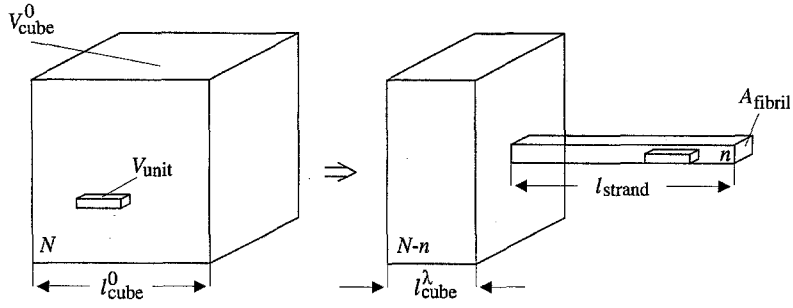

Fig. 1 Abstraction of the coil-strand-transition model: a coil (cube) is transformed into an isotropic rest coil (cube) and a highly oriented strand (fibril). V^0_{cube} is the volume of the initial cube, l^0_{cube} the length of the initial cube, V_{unit} the volume of a subunit, l^λ_{cube} the length of the rest cube, l_{strand} the length of the fibril, A_{fibril} the cross-section area of the fibril, N the number of subunits in the initial cube and n the number of subunits in the fibril

elastic properties. They concluded that hard elastic behavior cannot be based on lamellar deformations. Irrespective of the crystallinity a superstructure of oriented domains of fibrils parallel to the applied stress alternating with solid moieties is formed. Hard elastic behavior results from this bulk-fibril composite structure and the retractive force is mainly due to the properties of the fibrils. Using this, Chou et al. [24] computed the total restoring force on a fiber with an elastic and a surface tension component. Ren [25, 26] investigated the surface tension of fibrils, discussed the influence of internal friction and pointed out that hard elastic behavior of typical semi-crystalline polymers is a craze phenomenon. Experiments on thin films of high density polyethylene, which showed a behavior similar to that of hard elastic fibers, were done by Adams et al. [14]. Adams found that deformation initially occurs entirely in the intercrystalline regions, resulting in craze-like structures in the amorphous polymer layer between the lamellae. At higher strains the lamellae will be deformed (shear processes and block slip mechanisms) and partially destroyed.

As stated above, there seems to be a clear connection between hard elastic behavior and craze formation. Thus, we want to include in the introductory discussion of fibril formation in hard elastic materials at least the most prominent model for craze formation and propagation. Kramer and Berger, Plummer and Donald [27–30] explain fibril growth through a strain-softened non-Newtonian flow of the surrounding material into the fibril. The major contribution is due to scission and/or disentanglement of polymer chains during the movement into the fibril.

In this paper, we will investigate hard elastic polypropylene by x-ray scattering using a synchrotron radiation source and by performing stress strain measurements in different liquids. We compare our deformation measurements with predictions of the coil-strand-transition model. The coil-strand-transition model [31] is a new way to describe the deformation behavior of fibrillated materials, e.g., crazes [32]. In addition to the surface tension, it contains other energetic components as well as an entropic part.

First, we will explain in more detail the coil-strand-transition model.

Coil-strand-transition model

The description of the formation of fibrils with free volume is one of the objectives of the coil-strand-transition model. In the following part we will describe the model in brief. For more details see [31, 32]. Whereas many deformation models up to now start with affine transformations, the coil-strand-transition model is completely inhomogeneous. A polymer coil is not transformed into an ellipse during stretching, but forms an unoriented rest coil and a highly oriented strand (fibril). Figure 1 displays the model. The initial cube is filled with randomly distributed subunits. A subunit can be imaged as a Kuhn's segment with an associated volume. These subunits move into the strand. In the strand they are aligned in one direction.

It is possible to call the coil-strand-transition a phase transition. An unoriented state changes to an highly oriented state. As order parameter one could use Herman's orientation factor, which is zero before and finite afterwards. But it is not clear and not the purpose of the model to explain why the transformation occurs. This means that the transition might also be a non-equilibrium process, and then it is difficult to talk about a phase transition.

The introduced parameters in the model can all be physically interpreted. The model is not an ab initio model, but a static description of what happens with a given set of parameters.

The consequence of this above-described deformation behavior is that energy and entropy changes during stretching are linear with the elongation ratio λ as long as

the fibrils are growing.[1] The fundamental reason is that whenever a unit is transferred from the rest coil (rest cube) into the strand the same amount of energy or entropy is transferred. A detailed calculation results in

$$E^{CS} = N \cdot \Delta E \left(\frac{\lambda_{def} - 1}{\lambda_{fibril} - 1} \right) + E^{CS}_{surface} . \quad (1)$$

A similar formula holds for the entropy. We will not discuss the entropic part in this paper, because it can be shown that the contribution is minor [32, 33]. N is the number of subunits which fill the initial cube. ΔE denotes the energy change per subunit moving into the strand. ΔE contains contributions of elastic energy, trans-gauche transitions and chain scissions. λ_{def} is the elongation ratio of the deformation unit consisting of a rest cube (coil) and a strand (fibril).

$$\lambda_{def} = \frac{\text{length of strand } l_{strand} + \text{length of rest cube } l_{cube}}{\text{length of initial cube } l^0_{cube}} \quad (2)$$

λ_{fibril} is the natural draw ratio of the strand which is not changed during drawing. The interesting term for this paper is the energy stored in the created surface. It is given through

$$E^{CS}_{surface} = 2\gamma \, A_{fibril} \left((\lambda_{fibril} - 1)(1 - \delta_{\lambda def} 1) + 2\lambda^{3/2}_{fibril} \frac{\lambda_{def} - 1}{\lambda_{fibril} - 1} \right) . \quad (3)$$

γ is the surface tension and A_{fibril} is the cross-section of one strand (fibril). This is the energy due to one deformation unit. The Kronecker-delta takes care of the fact that no surface exists in the unstretched state. This sharp transition from no surface to a finite surface area is in accordance to observations in craze formation [34]. To get the total surface energy for a sample the whole created surface A must be calculated. The whole created surface A divided by the total amorphous volume $V_0(1 - \alpha)$ is equivalent to the surface of one coil-strand deformation unit divided by its volume V^0_{cube}. V_0 is the volume of the sample, α the degree of crystallinity. Thus, we get

$$\frac{A}{V_0(1-\alpha)} = \frac{2A_{fibril}}{V^0_{cube}} \left((\lambda_{fibril} - 1)(1 - \delta_{\lambda def} 1) + 2\lambda^{3/2}_{fibril} \frac{\lambda_{def} - 1}{\lambda_{fibril} - 1} \right) . \quad (4)$$

Since only the interlamellar regions are deformed $\varepsilon_{def} = \lambda_{def} - 1$ must be identified with the actual interlamellar extension $\varepsilon^* = \frac{\lambda - 1}{1 - \alpha}$ minus $\varepsilon^*_0 = \frac{\lambda_0 - 1}{1 - \alpha}$, the starting point of the coil-strand transition ($\lambda_0 \approx 1.03$–1.06, cf. Fig. 11). Thus, λ_{def} can be calculated from λ by

$$\lambda_{def} = \frac{\lambda - \lambda_0}{1 - \alpha} + 1 . \quad (5)$$

Using Eq. (5) and the following equation derived from the model

$$\frac{A_{fibril}}{V^0_{cube}} = \frac{1}{D_{fibril} \lambda^{3/2}_{fibril}} ,$$

we arrive at

$$E_{surface} = 2\gamma \frac{V_0}{D_{fibril}} \left(\frac{(\lambda_{fibril} - 1)(1 - \alpha)(1 - \delta_{\lambda 0} 1)}{\lambda^{3/2}_{fibril}} + 2 \frac{\lambda - \lambda_0}{\lambda_{fibril} - 1} \right) , \quad (6)$$

$E_{surface}$ being the energy due to the created surface in the whole sample.

Experimental

The samples used for the experiments were hard elastic polypropylene (HEPP) produced by Hoechst Celanese Corp., i.e., a precursor for Celgrad 2400 made of polypropylene MFR 1.15. The samples were films with an average thickness of 29 μm. DSC measurements resulted in a melting temperature of 174 °C, which is in accordance with the literature value for isotactic polypropylene [35]. The glass transition temperature of hard elastic (isotactic) polypropylene is between -10 °C and 15 °C [36]. With x-ray scattering we will try to detect the λ-range where the coil-strand-transition model can be applied. The prediction of the above outlined model will then be checked through varying the surface energy in HEPP with the help of two solvents. For the method see also [33]. All measurements were done at room temperature (20 °C).

x-ray scattering

Synchrotron radiation at DESY Hamburg was used to measure x-ray diffraction on-line to the deformation of the samples. This was done at the polymer beam line of HASYLAB. For this purpose the samples were stretched with an elongation ratio of 5% per minute, while the x-ray beam was focused on the center of the sample. Two

[1] Thus the refractive force, deduced from the free energy through differentiation, remains constant during the coil-strand formation.

Table 1 Relationship between scattering angles and displacement

Scattering angle [°]	0.05	0.1	0.15	0.2	0.25	0.3	0.35	0.4	0.45	0.5	0.6	0.7
Displacement [Å]	884	442	295	221	177	147	126	111	98	88	74	63

deformation cycles with a waiting time of 1 min between the cycles were done. The maximal elongation in the experiments was 40% and 80%. From the films specimens were cut with 10 cm length and 1 cm width. In Figs. 3–6 every scan line is the result of about 12 s of integration with a linear detector. All curves were smoothed using cubic splines. Table 1 lists the corresponding angle spacing value determined with CORNEA as reference sample. The data were correlated for primary beam intensity and thickness.

Stress-strain measurements

For the measurements in the different liquids specimens were cut with 50 mm length and 5 mm width. The specimens were deformed cyclically in air, methanol, and decalin to various draw ratios. The elongation ratio was 5% per minute. Neither swelling nor plasticizing effects were found for these liquids.

From these measurements the following quantities were evaluated: the work needed to deform the sample (area *ABCA* of Fig. 2), the immediately restored work (area *DBCD* of Fig. 2), the elastic recovery (the relation between *DC* and *AC*). The energy for the created surfaces were calculated by subtracting the curves in liquids from the corresponding curve in air.

Fig. 2 Sketch of a typical stress-strain curve of hard elastic material. The area *ABCA* is the work needed to deform the sample. The immediately resorted work is the area *DBCD*. The elastic recovery is defined by the ratio between *DC* and *AC*

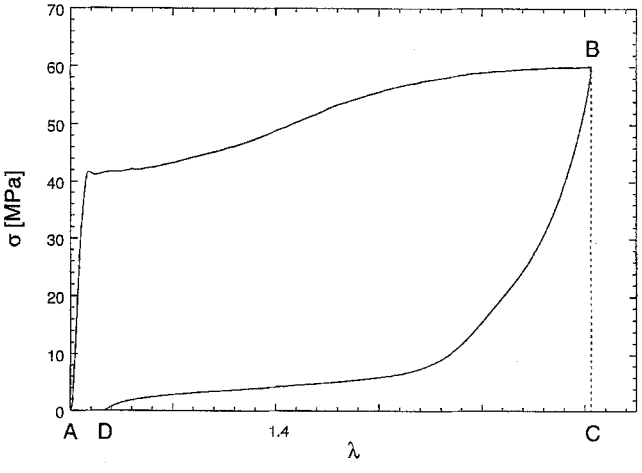

Table 2 Surface tension of different substances. The data are obtained from refs. [38] and [40]

Substance	γ [mJ/m^2]	γ^d [mJ/m^2]	γ^h [mJ/m^2]
Polypropylene [38]	30.2	30.2	0.0
Methanol [40]	23.0	22.0	1.0
Declain [40]	29.9	29.9	0.0

Table 3 Contact parameters of polypropylene with the liquids

Liquid	γ_{sL} [mJ/m^2]	$\gamma - \gamma_{sL}$ [mJ/m^2]
Methanol	1.7	28.5
Decalin	0.0007	~ 30.2

According to Fowkes, Owens and Wendt [37–39] the surface tension γ is divided into a contribution of dispersion forces γ^d and a contribution of hydrogen bonding forces γ^h:

$$\gamma = \gamma^d + \gamma^h . \tag{7}$$

The surface tension data for the polymer and liquids are listed in Table 2. The interfacial tension γ_{sL} of solid polymers ($\gamma_s = \gamma_s^d + \gamma_s^h$) in contact with liquids ($\gamma_L = \gamma_L^d + \gamma_L^h$) is given by [37–39]

$$\gamma_{sL} = \gamma_s + \gamma_L - 2\sqrt{\gamma_s^d \gamma_L^d} - 2\sqrt{\gamma_s^h \gamma_L^h} , \tag{8}$$

leading to Table 3, $\gamma - \gamma_{sL}$ being the compensated value.

Results and Discussion

In this section the results will be presented and discussed: in the first part our x-ray diffraction measurements, and in the second part our stress-strain measurements.

x-ray diffraction

For comparison with the x-ray scattering data a typical stress-strain curve of hard elastic polypropylene is shown in Fig. 2. After a short "Hookean" regime the specimen yields. The tension remains nearly constant up to about 30% to 40% elongation and then slightly increases once more.

Colloid & Polymer Science, Vol. 273, No. 11 (1995)

Previous work

In x-ray scattering [4, 41, 42] long periods in the meridian of about 140 Å were found. During stretching the long period increases to about 250 to 300 Å. At an elongation of about 30% to 40% a morphological change seems to take place [43]. In equatorial direction, Noether [4] found reflexes which he denoted to fibrils. Hosemann [41] showed that these fibrils have diameters of 50 Å, and the fibril spacing is about 120 Å. Wilke [44] tested the stability of the lamellae of annealed hard elastic polypropylene during elongation. He found that the dimensions of the lamellae change only very modestly, even at $\lambda = 2.3$. From this it can be concluded that lamellae are not destroyed up to draw ratios of about $\lambda = 2$. This is in agreement with Adams [14] who found that crystalline lamellae of annealed films do not deform until the strain in the amorphous region reaches about 300%. In contrast, lamellae of as extruded films break up at strain values of about 50%.

Obtained results

Figure 3 shows the meridian and Fig. 4 the equatorial scattering for the first and second cycle. Both the loading and unloading process are displayed. In Figs. 5 and 6 the first cycle for the deformation up to 80% is shown in a three-dimensional plot. All plots show a dramatic increase in scattered intensity during stretching. This is explainable through a large increase in electron contrast due to creation of voids in the sample.

The equatorial scattering shows a large decaying part which is essentially cut off by the beam stop, and a rather broad, but visible peak, sitting on the side of it. This is best seen in Fig. 6. This peak can be interpreted as fibril and void scattering starting at about the yield point ($\varepsilon \approx 5$–7%). The intensity becomes stronger and stronger with increasing λ, suggesting that more and more voids are formed. The data are compatible with a rather broad distribution of fibril spacings around 170 Å, a similar magnitude as discussed in the preceding section. The distribution is becoming smaller in the second cycle (Fig. 4), thus we suppose that the fibrils are formed more uniformly. The material seems to remember the former voids. Some smaller fibrils may coalesce.

The meridian displays a long period of the lamellae's spacing of about 140 Å with low intensity. This changes drastically in elongation as the electron contrast increases rapidly. Scattering from behind the beam stop becomes visible. The peak of the long period moves towards the beam stop, thus partially merging with the steep scattering cut off by the beam stop. The value of the long period reaches about 300 Å. Above 30% to 40% elongation this value of the long period and the intensity remains nearly constant. A relatively sharp change in the deformation behavior seems to take place which is nevertheless reversible to a large extent (cf. Fig. 3).

Due to the beam stop a discussion of the scattering close to the cutoff is not possible. Most likely, it is the result of large scale but isotropic density fluctuations.

These results are in good agreement with the previous work. The on-line data show that all changes occur rather quickly and are in large part reversible. The waiting time between first and second cycle was about 1 min. Nevertheless, the deformation is almost relaxed, even after stretching beyond 30–40%.

Morphological description

The following deformation model tries to cover all of the above-mentioned properties. While elongating the sample the lamellae separate from each other. After a short elastic regime a fibrillation of the amorphous interlamellar material takes place. The material yields and the voids as well as the fibril length increase. At about 30% to 40% elongation parts of the amorphous material reaches its natural draw limit. Some individual lamellae cannot move on anymore. Now, whole parts of the material begin to shear or shift against one another, perhaps bending other parts. Thus, the nearly constant lamellar spacing can be explained as well as the nearly unchanged dimensions of the lamellae. When unloading the sample, both the bended parts and the extended fibrils retract the lamellae, thus explaining the recovery, even for strains higher than typical for lamellae separation. A recrystallization of the lamellae could not be observed but may exist to a minor extent. The whole deformation behavior is sketched in Fig. 7.

Irreversible processes, which are present at all deformation stages, increase at strains higher than 30% to 40%. A combination of effects like pulling of fibrils out of lamellae [12, 22], plastic deformation processes [43], crystallization of fibrils [14, 16], lamellae deformation [14, 20] and destruction of small, not perfect lamellae [19, 42] are discussed. But they seem not to dominate in the regime up to 80%, because they should destroy the ability to retract the sample to a much higher extent.

Looking at this deformation behavior a regime between $\lambda \approx 1.1$ and $\lambda \approx 1.3 - 1.4$ can be found where fibril growth is the dominant part. In this regime the coil-strand-transition model should be applicable.

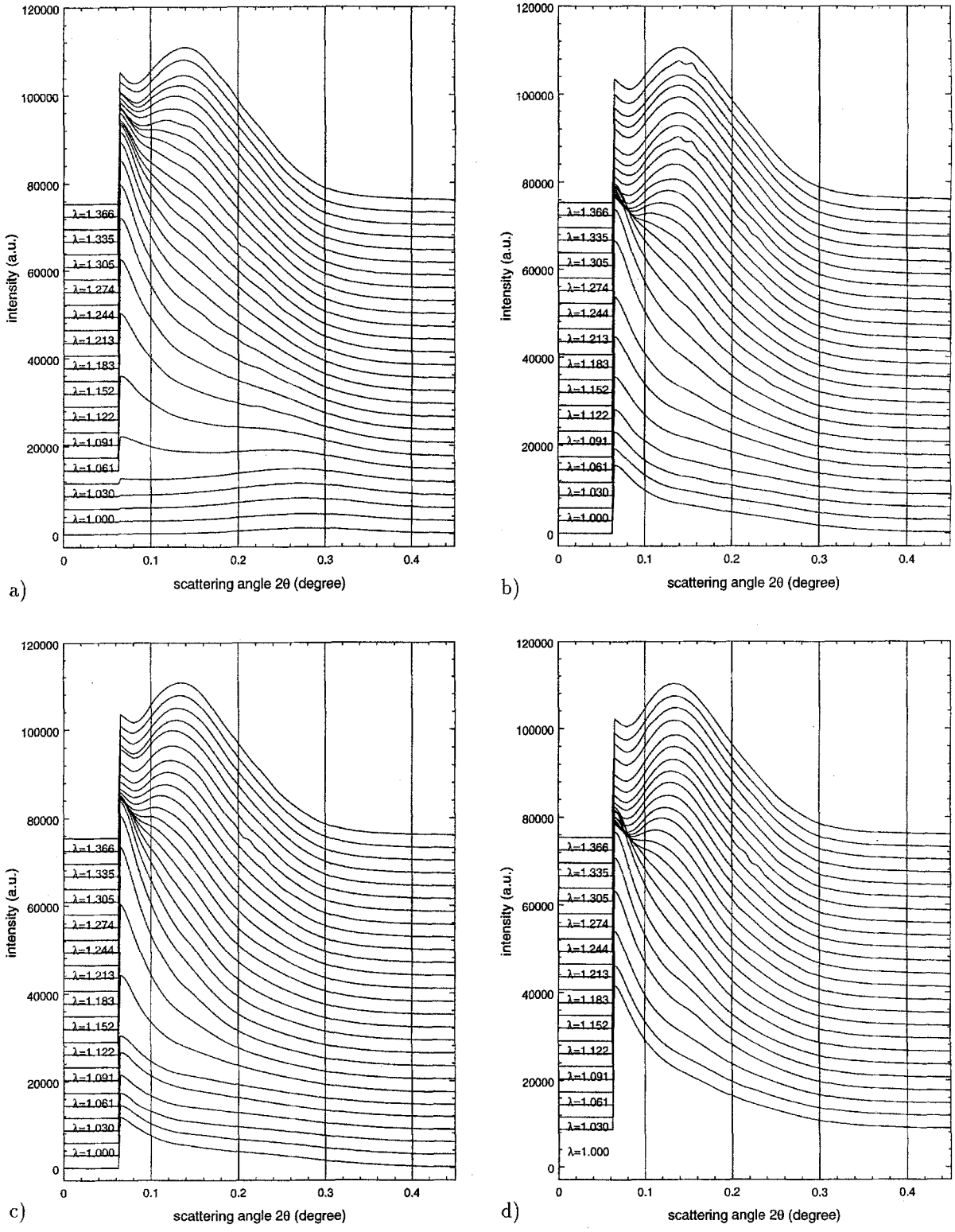

Fig. 3 Stacked plots of meridional x-ray scattering of HEPP: a) first cycle: stretching b) first cycle: unloading c) second cycle: stretching d) second cycle: unloading

Colloid & Polymer Science, Vol. 273, No. 11 (1995)

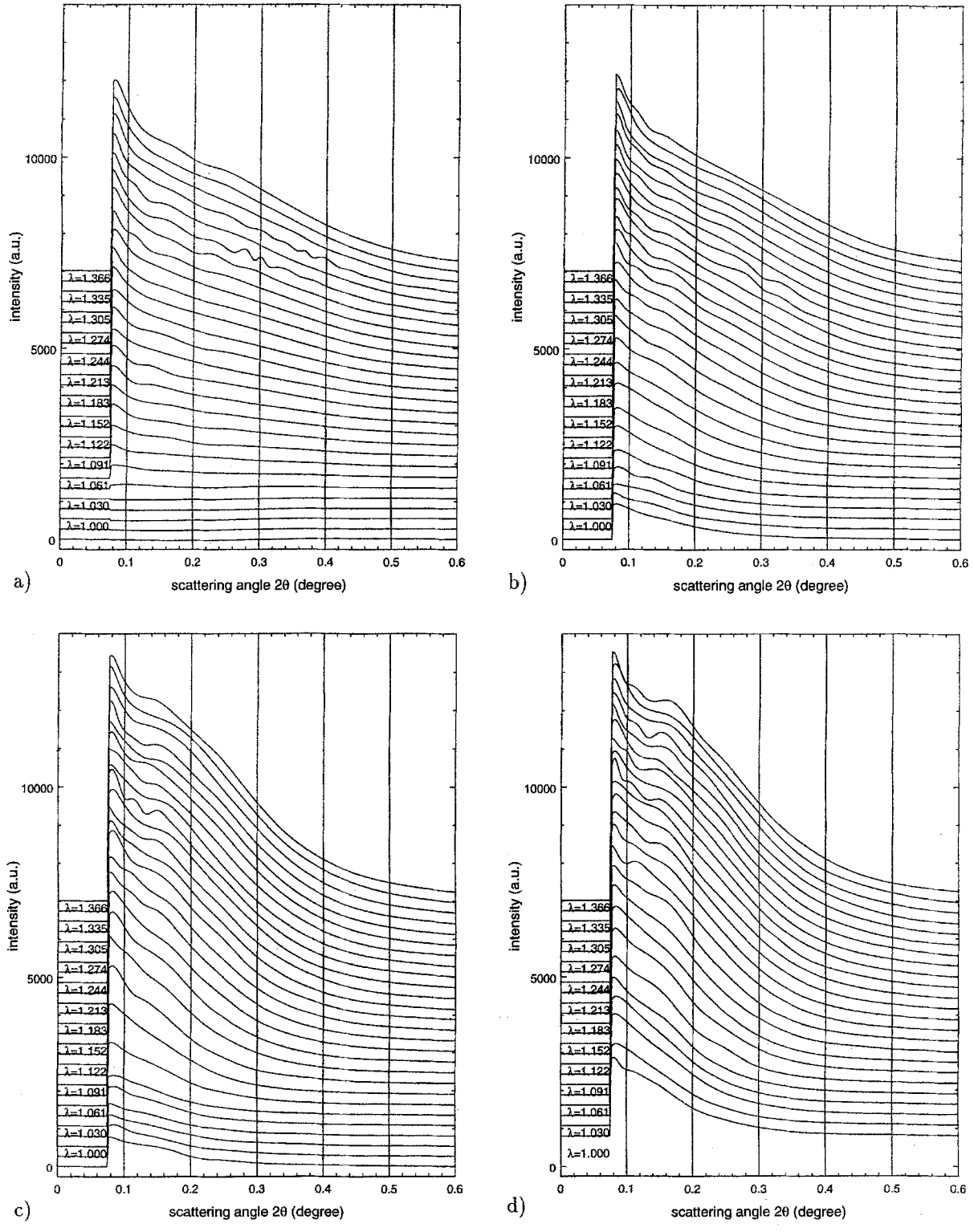

Fig. 4 Stacked plots of equatorial x-ray scattering of HEPP: a) first cycle: stretching b) first cycle: unloading c) second cycle: stretching d) second cycle: unloading

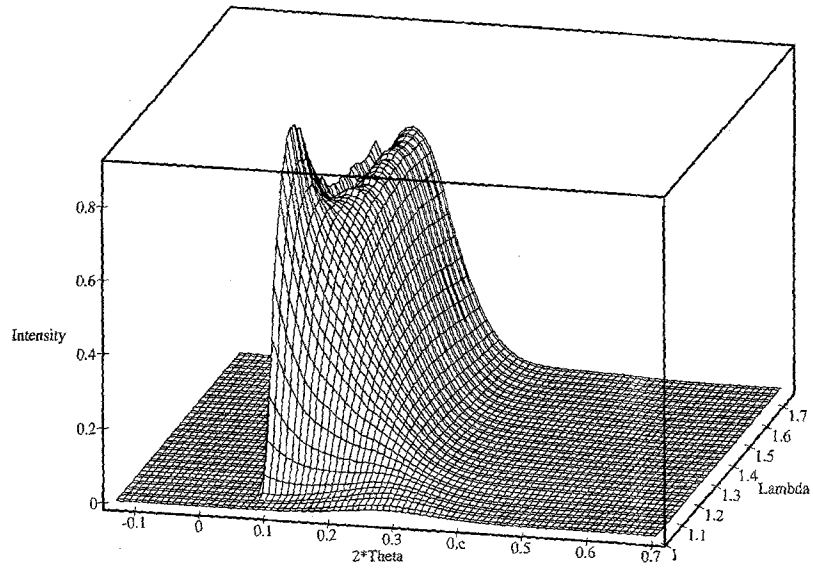

Fig. 5 Three-dimensional plot of meridional x-ray scattering of HEPP, stretched up to $\lambda = 1.8$

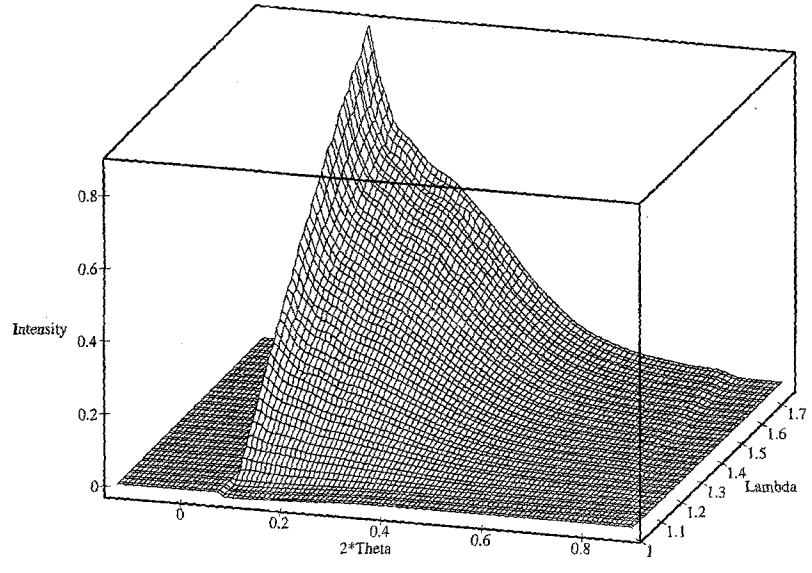

Fig. 6 Three-dimensional plot of equatorial x-ray scattering of HEPP, stretched up to $\lambda = 1.8$

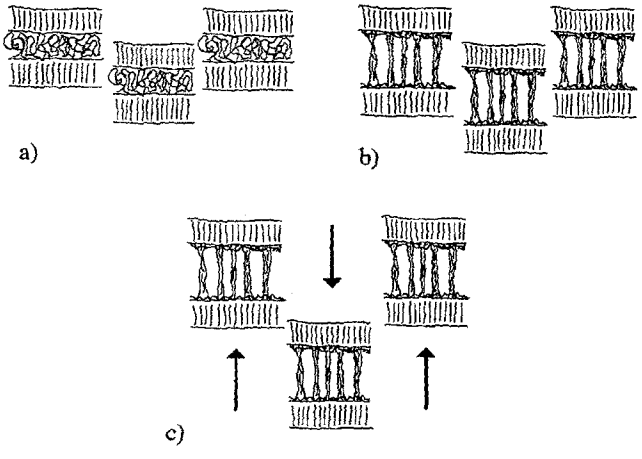

Stress-strain measurements

Part of the deformation curves of the first and second cycle in the different liquids are shown in Figs. 8, 9, 10. The results of work/energy evaluations from the measurements are displayed in Figs. 11 to 14.

These figures will be described and discussed in the next paragraphs.

Fig. 7 Sketch of the deformation considerations for HEPP: a) undeformed state: lamellae with amorphous material in between b) regime $\lambda \approx 1.1$ up to $\lambda \approx 1.4$: the lamellae are separating, fibrils are formed c) regime $\lambda > 1.4$: the deformation of the interlamellar material is nearly stopped, larger parts are shifted or bended

Colloid & Polymer Science, Vol. 273, No. 11 (1995)

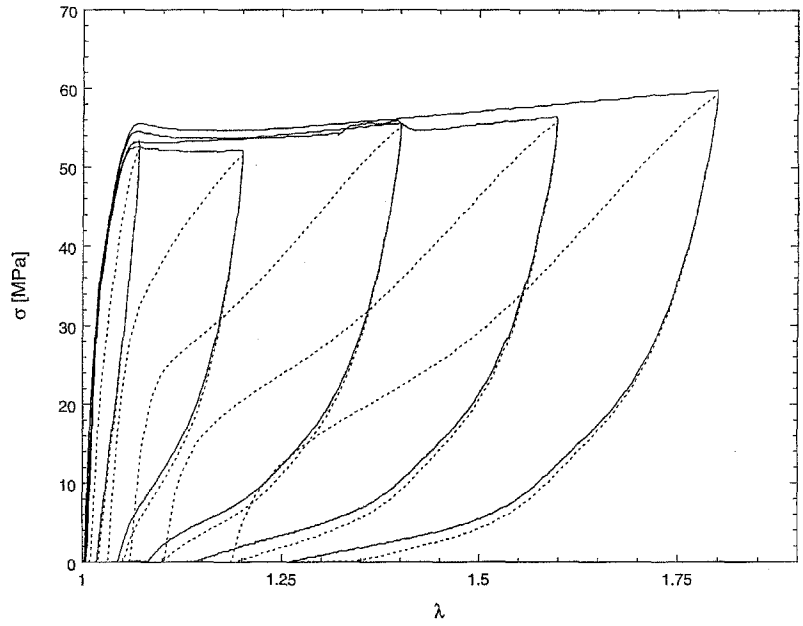

Fig. 8 Stress-strain curves for HEPP, first (solid lines) and second (dotted lines) cycle, strained in air

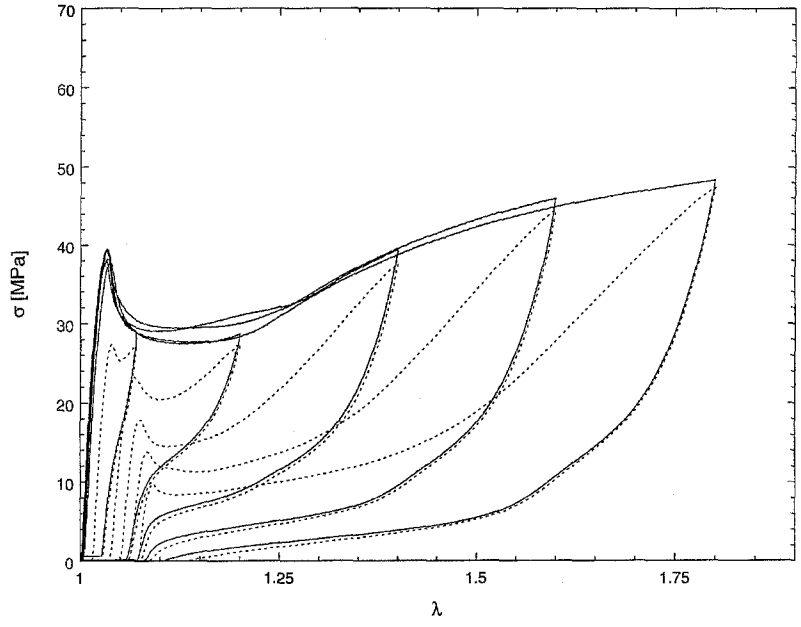

Fig. 9 Stress-strain curves for HEPP, first (solid lines) and second (dotted lines) cycle, strained in methanol

Before yielding

Prevorsek et al. [45] mentioned great hysteresis losses even at low strain ratios in cyclic stress strain measurements. We can confirm their results well below the yield transition. The "Hookean" regime seems to end after only 3–4% of stretching (cf. inserts of Figs. 11, 12, 13), whereas the yield point in air is at about 7%. It would be of interest whether the hysteresis is dependent on the deformation speed, but we performed all measurements with an elongation ratio of 5% per minute.

The fibril formation seems to start after the Hookean part, but before the yield point. This should be reflected in the curves within liquids. The yield point in methanol shows a clear shift to a lower value. The already penetrating methanol decreases the energy needed for yielding, thus leading to an earlier yield point at a diminished stress. In contrast to that the decalin curves behave almost

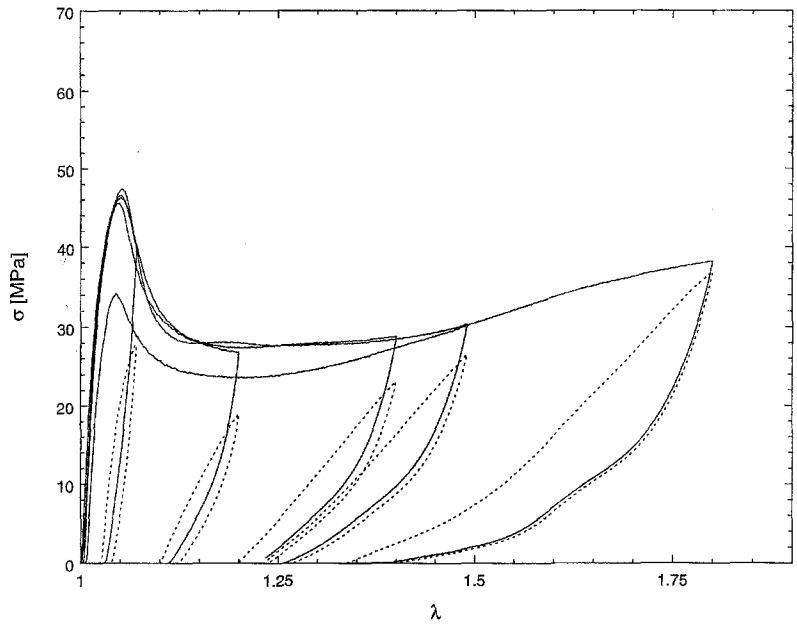

Fig. 10 Stress-strain curves for HEPP, first (solid lines) and second (dotted lines) cycle, strained in decalin

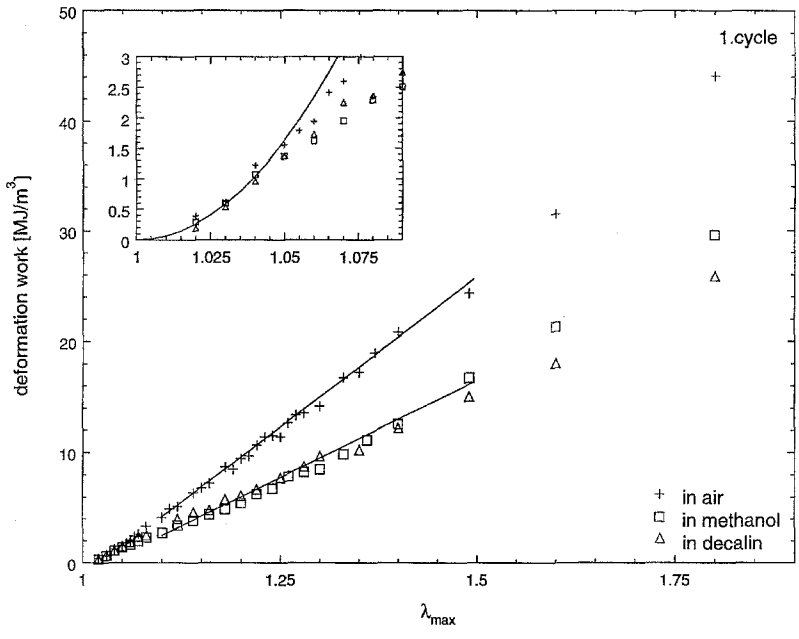

Fig. 11 The deformation work per volume versus λ_{max}, deduced from area $ABCA$ of Fig. 2: first cycle

identical to the curves in air up to the yield point. The yield tension is nearly the same as in air. This is surprising, since the possibility of compensating the surface energy is even better than that of methanol (cf. Table 3). We relate this to the significantly larger molecular structure of the decalin in its all chair conformation (mean diameter about four times as large as of methanol [46]). Thus decalin is not able to penetrate into HEPP before the material undergoes the yield process. The first created holes are too small. After yielding the curves in decalin decrease more sharply and much more than the methanol curves. The final value of the stress in the range of $\lambda \approx 1.1$ up to $\lambda \approx 1.3$ is thus nearly the same in both liquids. This is now in accordance to the values of Table 3 where both liquids reduce the surface tension almost totally. When unloading the samples the stored work is relieved to some extent. Once more decalin shows a peculiar result. The elastic recovery (Fig. 15) as well as the restored work (Fig. 13) is much

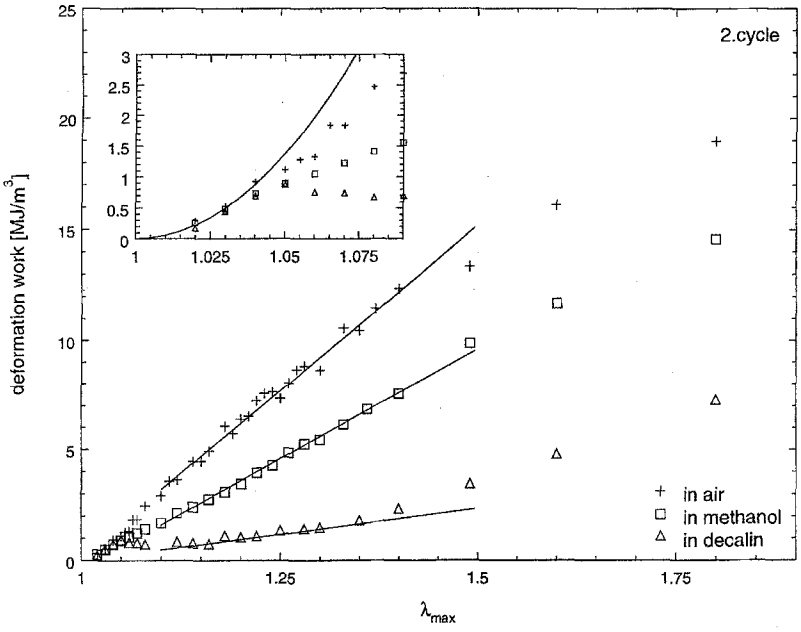

Fig. 12 The deformation work per volume versus λ_{max}, deduced from area *ABCA* of Fig. 2: second cycle

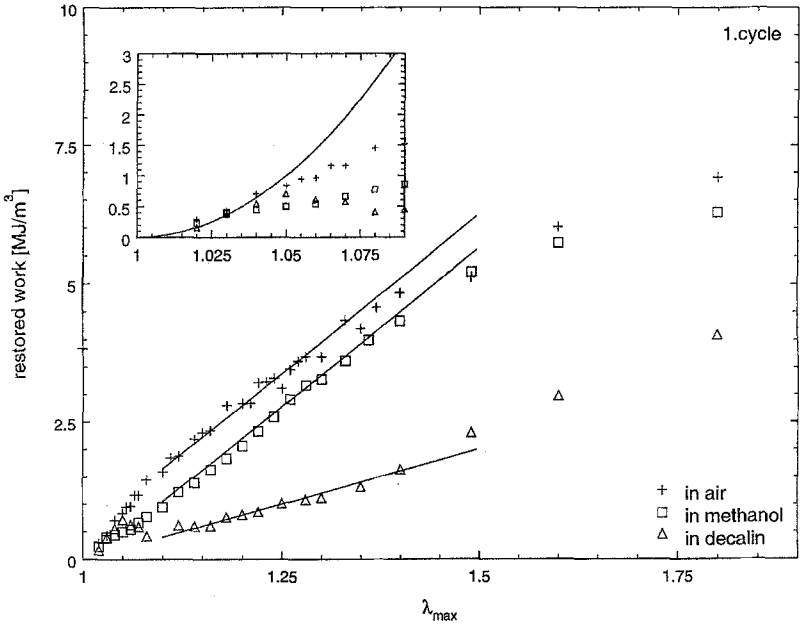

Fig. 13 The restored work per volume versus λ_{max}, produced during unloading, deduced from area *DBCD* of Fig. 2: first cycle

lower than for methanol and air. It seems as if the large decalin molecule is not able to leave the material in the time available. It is trapped in the collapsing voids whereas methanol is able to use the smaller holes to get out of the material. This can also be seen in the second cycle of the deformation curves Fig. 10.[2]

The coil-strand-transition regime

The stress-strain-curves of methanol and decalin show that after the drop of the stress at the yield point the stress remains quite constant up to $\lambda \approx 1.3 - 1.4$. This regime should be the regime of fibril growth as shown in the x-ray

[1] Thus the refractive force, deduced from the free energy through differentiation, remains constant during the coil-strand formation.

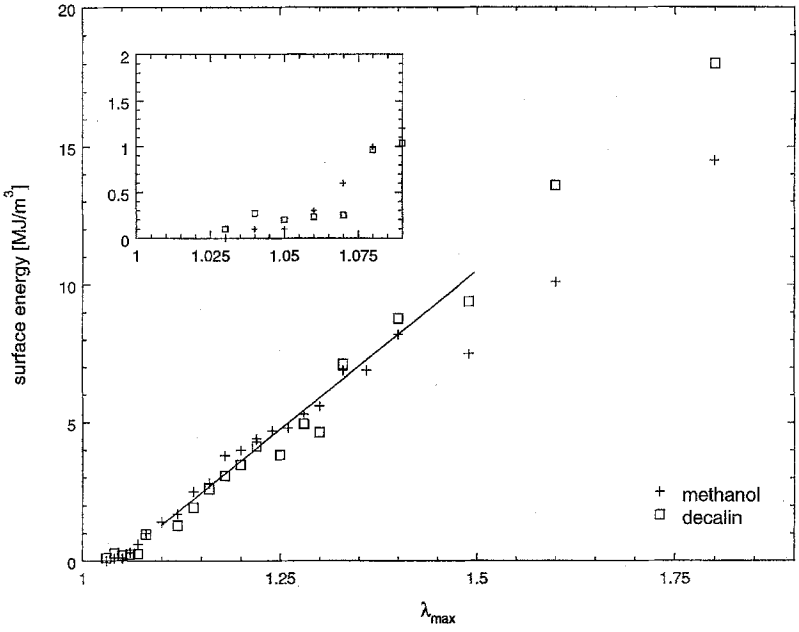

Fig. 14 The energy due to the formation of internal surfaces versus λ_{max}, deduced through substraction of the curves of Fig. 9, Fig. 10 from the curves of Fig. 8

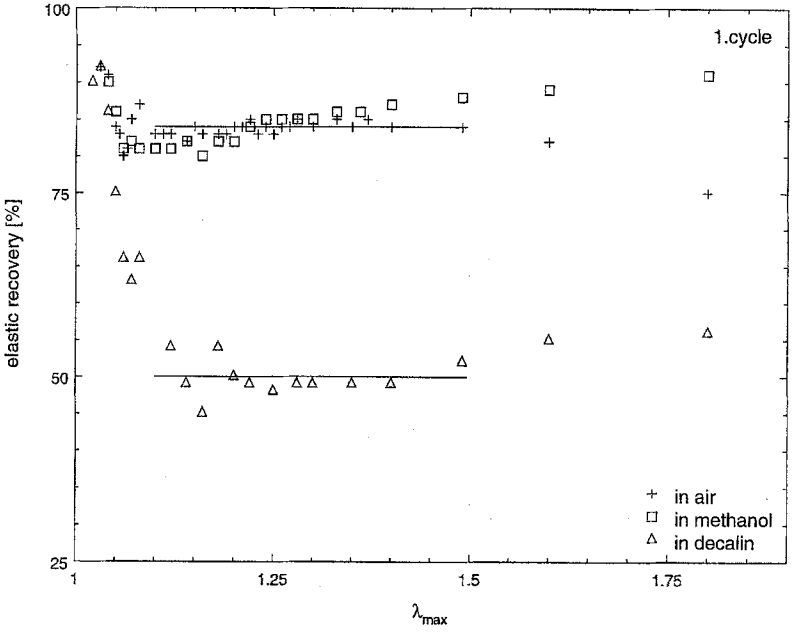

Fig. 15 The elastic recovery deduced from the ratio *DC/AC* (cf. Fig. 2)

scattering. The stress level is controlled by fibril growth according to the coil-strand-transition model and some dynamic contributions, i.e., internal friction [25]. Beyond $\lambda \approx 1.3 - 1.4$ additional new processes start as mentioned above. Thus the range $\lambda \approx 1.1$ up to $\lambda \approx 1.4$ should be the range where the coil-strand-transition model should be applicable. The straight lines in the plots 11, 12 and 13 clearly show the proposed linear relationship between work and elongation. The linear relationship of the work is in agreement with deformation-calorimetric measurements on hard elastic polypropylene [16].

The linear relationship is valid also for the second cycle although the stress-strain-curves are not linear in this regime. The sample remembers the predeformed state and forms once more a coil and a strand (fibril). The length of the fibril is so directly related to the achieved length of the sample in the cyclic experiment and thus the work is linear to that length. The stress in the second cycle is lower than

in the first cycle (up to the maximal elongation where the stresses are equal). This is due to the fact that the amorphous regions are pre-oriented [16]. The entanglement density is lower, less chain scissions occur and internal friction is reduced. The yield peak in methanol indicates that during recovery methanol is leaving the sample, and subsequent stretching results in a new formation of fibrils and voids.

The compensated surface energy (Fig. 14) shows this linear relation, too. The energy is the same for both liquids, in accordance with the data of Table 3.

Surface energy

In the last section we want to check whether the coil-strand-transition-model is able to predict the amount of the surface energy in the correct range.

For $\lambda = 1.3$ the deformation work per unit volume W_{def} is 14.2 MJ/m^3 (cf. Fig. 11). The volume of the sample is $V_0 = 7.25 \cdot 10^{-9}$ m^3. Thus the deformation work $W = W_{def} \cdot V_0 \approx 106$ mJ. With typical values for $D_{fibril} = 4$ nm [24], $\lambda_{fibril} = 4$ [28], a surface tension of $\gamma = 30.2$ mJ/m^2, a crystallinity α of about 0.5 ± 0.1, we get for $E_{surface}$ (Eq. (6)) in the coil-strand-transition model for $\lambda = 1.3$ a value of (41 ± 4) mJ. Thus the ratio between $E_{surface}$ and W is (39 ± 4) %. If we take the values from Fig. 14 and Fig. 11 the ratio is (37 ± 4) %, which is in good agreement with the theoretical prediction. The ratio of about one-third is also in good agreement to measurements on crazes, a closely related topic [27, 32].

Conclusion

In the range of $\lambda \approx 1.1$ up to $\lambda \approx 1.3 - 1.4$ fibril growth is the dominating deformation mechanism of hard elastic polypropylene. In this regime the long period increases with the elongation from 140 to 300 Å. The fibril spacing shows a broad distribution around 170 Å. At higher strains ($\lambda > 1.4$) a change in the deformation behavior takes place and other deformation processes are involved, too. They are a combination of effects like pulling of fibrils out of lamellae [12, 22], plastic deformation processes [43], crystallization of fibrils [14, 16], lamellae deformation [14, 20], destruction of small and not perfect lamellae [19, 42]. We added to these processes a shifting and shearing of whole parts of material against one another which increase the restorative possibility of the samples.

The coil-strand-transition model is able to describe the linear relationship between the deformation work as well as the surface energy and the elongation in the range of $\lambda \approx 1.1$ up to $\lambda \approx 1.3 - 1.4$. Furthermore, the calculated ratio between the surface energy and the deformation work is in good agreement with the measurements.

Acknowledgement We wish to thank DESY Hamburg and Prof. Zachmann for the measuring time to perform the x-ray scattering experiments.

References

1. British Patent (1964) (to Canadian Celanese Ltd.), July 1, 962:231
2. Noether HD, Whitney W (1973) Kolloid Z. u. Z. Polym. 251:991
3. Park IK, Noether HD (1975) Colloid Polym Sci 253:824
4. Noether HD, Brody H (1976) Textile Research Journal 46(7):467
5. Noether HD, Hay IL (1978) J Appl Cryst 11:546
6. Garber CA, Clark ES (1970) J Macromol Sci-Phys B4(3):499
7. Clark ES (1973) Structure and Properties of Polymer Films, edited by R.W. Lenz and R.S. Stein, Plenum, New York
8. Quynn RG, Brody H (1971) J Macromol Sci-Phys B5:721
9. Sprague BS (1973) J Macromol Sci-Phys B8:157
10. Cannon SL, McKenna GB, Statton WO (1976) J Polym Sci – Macromol Rev 11:209
11. Cayrol B, Petermann J (1974) J Polym Sci Polym Phys 12:2169
12. Miles M, Petermann J, Gleiter H (1976) J Macromol Sci-Phys B12:523
13. Gohil RM, Petermann J (1979) J Polym Sci Polym Phys 17:525
14. Adams WW, Yang D, Thomas EL (1986) J Mater Sci 21:2239
15. Göritz D, Müller FH (1974) Coll Polym Sci 252:862
16. Göritz D, Müller FH (1975) Coll Polym Sci 253:844
17. Wool RP (1976) J Polym Sci Polym Phys 14:603
18. Hosemann R, Loboda-Čačhović J, Čačhović H (1976) Coll Polym Sci 254:782
19. Čačhović H, Loboda-Čačhović J, Hosemann R, Göritz D (1979) J Macromol Sci Phys B16(1):145
20. Hashimoto T, Nagatoshi K, Todo A, Kawai H (1976) Polymer 17:1063
21. Ishikawa H, Numa H, Nagura M (1979) Polymer 20:516
22. Miles MJ, Baer E (1979) J Mater Sci 14:1254
23. Moet A, Palley I, Baer E (1980) J Appl Phys 51(10):5175
24. Chou CJ, Hilter A, Baer E (1986) Polymer 27:369
25. Ren W (1992) Coll Polym Sci 270:943
26. Ren W (1992) Coll Polym Sci 270:990
27. Kramer EJ (1983) Adv Polym Sci 52/53:2
28. Berger LL, Buckley DJ, Kramer EJ, Brown HR, Bubeck RA (1987) J Polym Sci 25:1679
29. Kramer EJ, Berger LL (1990) Adv in Polym Sci 91/92:1
30. Plummer CJG, Donald AM (1990) Macromolecules 23:3929
31. Göritz D, Kreitmeier S, Wittkop M, J Macromol Sci-Phys, submitted
32. Kreitmeier S, Göritz D (1991) Makromol Chem Macromol Symp 41:253

33. Wittkop M, Kreitmeier S, Göritz D (1995) Acta Polymerica 46:319
34. Michler GH, private communication
35. Brandrup J, Immergut EH (1989) Polymer Handbook, Third Edition, New York, London, Sydney, Toronto
36. Göritz D (1978) Habilitationsschrift, Universität Ulm
37. Fowkes FM (1964) Ind Engr Chem 56:40
38. Owens DK, Wendt RC (1969) J Appl Polym Sci 13:1741
39. Owens DK (1970) J Appl Polym Sci 14:1725
40. van Krevelen DW (1976) Properties of Polymers, Amsterdam, Oxford, New York
41. Hosemann R, Čačhović H (1981) Colloid Polym Sci 259:15
42. Hosemann R, Schulze I (1987) Colloid Polym Sci 265:686
43. Samuels RJ (1979) J Polym Sci Polym Phys 17:535
44. Wilke W (1979) Coll Polym Sci 257:101
45. Prevorsek C, Shama RK, Kwon YD (1982) Polymer Preprints 19:332
46. Mayer A, Chemistry Department, University of Regensburg, private communication